

THE LCO/PALOMAR 10,000 km s⁻¹ CLUSTER SURVEY. II.
CONSTRAINTS ON LARGE-SCALE STREAMINGJEFFREY A. WILLICK¹

Department of Physics, Stanford University, Stanford, CA 94305-4060

E-mail: jeffw@perseus.stanford.edu

Submitted to the Astrophysical Journal

ABSTRACT

The LCO/Palomar 10,000 km s⁻¹ (LP10K) Tully-Fisher (TF) data set is used to test for bulk streaming motions on a $\sim 150h^{-1}$ Mpc scale. The sample consists of 172 cluster galaxies in the original target range of the survey, 9000–13,000 km s⁻¹ redshift, plus an additional 72 galaxies with $cz \leq 30,000$ km s⁻¹. A maximum-likelihood analysis that is insensitive to Malmquist and selection bias effects is used to constrain the bulk velocity parameters, and realistic Monte-Carlo simulations are carried out to correct residual biases and determine statistical errors. When the analysis is restricted to the original target range, the bias-corrected bulk flow is $v_B = 720 \pm 280$ km s⁻¹ (1σ error) in the direction $l = 266^\circ$, $b = 19^\circ$, with an overall 1σ directional error of 38° . When all objects out to $z = 0.1$ are included the result is virtually unchanged, $v_B = 700 \pm 250$ km s⁻¹ toward $l = 272^\circ$, $b = 10^\circ$ with a directional uncertainty of 35° . The hypothesis that the Hubble flow has converged to the CMB frame at distances $\lesssim 100h^{-1}$ Mpc is ruled out at the 97% confidence level. The data are inconsistent with the flow vector found by Lauer & Postman; though similar in amplitude, the LP10K and Lauer-Postman flow vectors are nearly orthogonal. However, the LP10K bulk flow is consistent with that obtained from the SMAC survey of elliptical galaxies recently described by Hudson *et al.* If correct, the LP10K results indicate that the convergence depth for the Hubble flow is $\gtrsim 150h^{-1}$ Mpc. However, the modest statistical significance of these results, together with contrasting claims recently made in the literature, suggest that further observational data are required before firm conclusions are drawn.

1. INTRODUCTION

For the past decade, establishing the scale of the largest bulk flows has been one of the major goals of observational cosmology. In the late 1980s, the “7-Samurai” (7S) group used the D_n - σ relation² to show that the peculiar velocity field in the nearby universe, $cz \lesssim 4000$ km s⁻¹, is dominated by a coherent, large-amplitude ($v_B \approx 500$ km s⁻¹) bulk motion in the direction of the “Great Attractor” (GA) near $l = 310^\circ$, $b = 10^\circ$ (Dressler *et al.* 1987; Lynden-Bell *et al.* 1988). Willick (1990) obtained Tully-Fisher (TF) data for a sample of over 300 field spirals, and found that the Perseus-Pisces supercluster, at a distance of $\sim 50h^{-1}$ Mpc and on the opposite side of the sky at $l \sim 110^\circ$, $b \sim -30^\circ$, moves in the same direction as the 7S ellipticals at a velocity of ~ 400 km s⁻¹. A similar result was obtained by Han & Mould (1992) from a cluster TF sample in Perseus-Pisces. Mathewson *et al.* (1992) analyzed over 1300 Southern-sky TF spirals, and found that the flow identified by the 7S continued beyond the GA, because spirals in the GA region itself were moving rapidly away from the Local Group (LG). Courteau *et al.* (1993) used a preliminary version of the Mark III Catalog of Galaxy Peculiar Velocities (Willick *et al.* 1997a) to measure the bulk flow for the entire volume within $60h^{-1}$ Mpc, finding $v_B = 360 \pm 40$ km s⁻¹ toward $l = 294^\circ$, $b = 0^\circ$. A recent reanalysis of the Mark III Catalog using the POTENT method by Dekel *et al.* (1998) finds $v_B = 370 \pm 110$ km s⁻¹ toward $l = 305^\circ$, $b = 14^\circ$ for the volume within $50h^{-1}$ Mpc.

Thus, TF and FP data sets acquired through the early 1990s agreed on the reality of coherent bulk flows within $\sim 50h^{-1}$ Mpc. These motions were measured relative to the reference frame in which the dipole anisotropy of the Cosmic Microwave Background (CMB) vanishes, henceforward the “CMB” frame. The LG itself moves with a velocity of 627 km s⁻¹ toward $l = 276^\circ$, $b = 30^\circ$ in the CMB frame (Kogut *et al.* 1993). This direction is within 30 – 40° of the observed bulk flows, suggesting that the LG motion itself is generated, at least in part, on $\gtrsim 50h^{-1}$ Mpc scales.

The studies cited above were not, however, deep enough to establish whether the bulk flows ended, or converged, beyond $50h^{-1}$ Mpc. Evidence of nonconvergence beyond this distance was first provided by the work of Lauer & Postman (1994, LP94), who used brightest cluster galaxies (BCGs) as a distance indicator. LP94 analyzed a sample of 119 BCGs out to a distance of 15,000 km s⁻¹, and concluded that the entire volume out to that distance was moving coherently at ~ 700 km s⁻¹ in the direction $l = 343^\circ$, $b = 52^\circ$. This flow vector was about 60° away from the motions detected in the earlier FP and TF-based studies, and was on a much larger scale.

However, a number of recent studies have challenged the validity of both the LP94 result in particular, and very large-scale ($\gtrsim 100h^{-1}$ Mpc) bulk flows in general. Giovanelli *et al.* (1996) analyzed a large sample of TF spirals toward the apex and antapex of the LP94 flow direction, and found zero net peculiar velocity along that axis out

¹Cottrell Scholar of Research Corporation² D_n - σ is one example of a class of elliptical galaxy scaling relations known as the Fundamental Plane (FP). We adopt the latter term for the remainder of the paper.

to a distance of $\sim 70h^{-1}$ Mpc. Riess, Press, & Kirshner (1995) used 13 Supernovae of Type Ia (SN Ia), each with a distance error less than 10%, to constrain the magnitude and direction of the bulk flow within $10,000 \text{ km s}^{-1}$ redshift. They showed that their data set was inconsistent with the LP94 flow vector at 99% confidence. More recently, Giovanelli *et al.* (1998a,b) and Dale *et al.* (1998) have analyzed I-band field and cluster TF samples to estimate the convergence scale. Giovanelli (1998a,b) found convergence at $\lesssim 6000 \text{ km s}^{-1}$ using primarily field spirals. Dale *et al.* (1998) combined the distant ($cz > 4500 \text{ km s}^{-1}$) portion of the Giovanelli (1998a,b) sample with 522 spirals in 52 Abell clusters at distances between ~ 50 and $\sim 200h^{-1}$ Mpc. The effective depth of this combined sample was $\sim 9500 \text{ km s}^{-1}$. Dale *et al.* found a bulk velocity consistent with zero, and at most 200 km s^{-1} , for this volume. The EFAR group (Wegner *et al.* 1996, 1998) has obtained FP data for ~ 500 ellipticals in 84 clusters in two patches of the sky. They also find generally small cluster peculiar velocities in the mean, and in particular rule out the LP flow at 99% confidence (Saglia *et al.* 1998). However, the limited sky coverage of the EFAR sample means that it is not sensitive to the full range of possible flow directions.

In contrast, the recently completed SMAC survey of elliptical galaxies (Hudson *et al.* 1998a,b) has found evidence for a large-scale bulk flow, though not in the LP94 direction. The SMAC group measured FP distances for 697 early-type galaxies in 56 clusters with $cz \leq 12,000 \text{ km s}^{-1}$, and found a bulk flow of $640 \pm 200 \text{ km s}^{-1}$ in the direction $l = 260 \pm 15^\circ$, $b = -1 \pm 12^\circ$. This flow vector is within $40\text{--}50^\circ$ of, and is similar in amplitude to, the motions detected 5–10 years ago by the 7S, Willick (1990), Mathewson *et al.* (1992), and Courteau *et al.* (1993). However, the SMAC data set has about twice the effective depth of those earlier surveys, and thus suggests that the convergence scale could be $\gtrsim 8000 \text{ km s}^{-1}$.

In short, while a number of studies agree on the reality of a significant bulk flow within $50h^{-1}$ Mpc, the persistence of such motions to distances beyond $\sim 80h^{-1}$ Mpc remains controversial. The purpose of this paper is to address this issue using a new data set. The outline of the paper is as follows. In § 2, we describe the new TF data set, known as the LP10K sample. In § 3, we describe the maximum-likelihood method used to constrain the bulk flow vector. In § 4, we apply this method to the LP10K data set. In § 5, we describe Monte-Carlo simulations of the sample, and discuss how these simulations are used to assess the statistical significance of the results. Finally, in § 6 we further discuss and summarize the main results of the paper.

2. THE LP10K SURVEY

In early 1992 the author initiated a survey designed specifically to test whether the bulk streaming observed within $50\text{--}60h^{-1}$ Mpc persists to distances $\gtrsim 100h^{-1}$ Mpc. The survey targeted spiral and elliptical galaxies in 15 Abell clusters with published redshifts in the range $9000 \leq cz \leq 12,000 \text{ km s}^{-1}$, and utilized the TF and FP relations as distance indicators.³ To maximize sensitivity to a

bulk flow, the 15 clusters were selected to be distributed as isotropically as possible on the sky. Limitations to isotropy were imposed only by the requirement of Galactic latitude $|b| \geq 20^\circ$ to minimize extinction effects and by the finite number of clusters observed. Southern-sky clusters were observed from the Las Camapanas Observatory (LCO), while Northern-sky clusters were observed from Palomar Observatory. The survey is thus known as the LCO/Palomar 10,000 km s^{-1} Cluster Survey (LP10K).

The LP10K observing runs spanned the period 1992 March–1995 September, and totaled over 100 nights of observations. The observing strategy, data reduction methods, and the modeling of the TF relation were described in detail by Willick (1999a), hereafter Paper I. Although the LP10K TF data set is fully analyzed, observations and reductions of the elliptical galaxy portion of the survey are ongoing, with completion expected in 2–3 years. *The results presented here are derived from TF data only.* The full TF data set, along with a variety of tests of the accuracy and repeatability of the observations, will be presented in the third paper in this series (Willick 1999b, Paper III).

Figure 1 shows the sky positions of the 15 LP10K clusters in Galactic coordinates. (The equatorial coordinates of the clusters are listed in Table 1 of Paper I.) The clusters are seen to be well distributed around the sky above $|b| = 20$. There are clusters near both the apex and the antapex of the CMB dipole at $l = 276^\circ$, $b = 30^\circ$, ensuring sensitivity to flows along this axis. The axis corresponding to the LP94 motion is similarly well-sampled. An unexpected feature of the survey, discussed in Paper I, was that many TF galaxies turned out to have redshifts well in excess of the published cluster velocities. To appreciate the extent of this effect, Figure 1 indicates the mean redshift $\langle cz \rangle$ of each cluster TF sample by point type: solid circles indicate mean redshifts in the original target range, $\langle cz \rangle \leq 12,000 \text{ km s}^{-1}$ (in practice all of these have $\langle cz \rangle > 11,000 \text{ km s}^{-1}$ as well); open circles show clusters with $12,000 < \langle cz \rangle \leq 15,000$; and starred symbols clusters with $\langle cz \rangle > 15,000 \text{ km s}^{-1}$. It is apparent that a sizable *majority* of LP10K sample clusters have mean redshifts greater than $12,000 \text{ km s}^{-1}$, the upper limit of the original target range. Indeed, the sample includes a significant number of objects with $z \simeq 0.1$. The number of TF galaxies per cluster is denoted by point size. The cluster TF sample sizes range from 8 to 26 objects, with an average of about 16 galaxies per cluster.

Table 1 provides additional information on the cluster TF samples. Column 1 gives the cluster name according to the catalogue of Abell, Corwin, & Olowin (1989; ACO). Columns 2 and 3 give the cluster Galactic coordinates l and b . There follows a listing of three redshifts for the cluster: column 4 lists an updated value derived from a literature search, typically weighted by early-type galaxies in the cluster core; column 5 lists the mean redshift of all LP10K TF galaxies in the cluster field; and column 6 lists the mean sample redshift when only objects with $7000 \leq cz \leq 15,000 \text{ km s}^{-1}$ are included (the significance of this redshift cut is discussed below). All redshifts are given with respect to the CMB frame. Column 7 lists the total number of TF galaxies in each cluster field; these values

³As discussed below, the upper end of the redshift range for these clusters turns out to be closer to $13,000 \text{ km s}^{-1}$, the value quoted in the Abstract.

correspond to the point sizes in Figure 1 as well as the redshifts in column 5. Column 8 lists the number of galaxies with $7000 \leq cz \leq 15,000 \text{ km s}^{-1}$ and correspond to the redshift in column 6. Column 9 provides keys to the sources from which the literature-based redshift are derived.

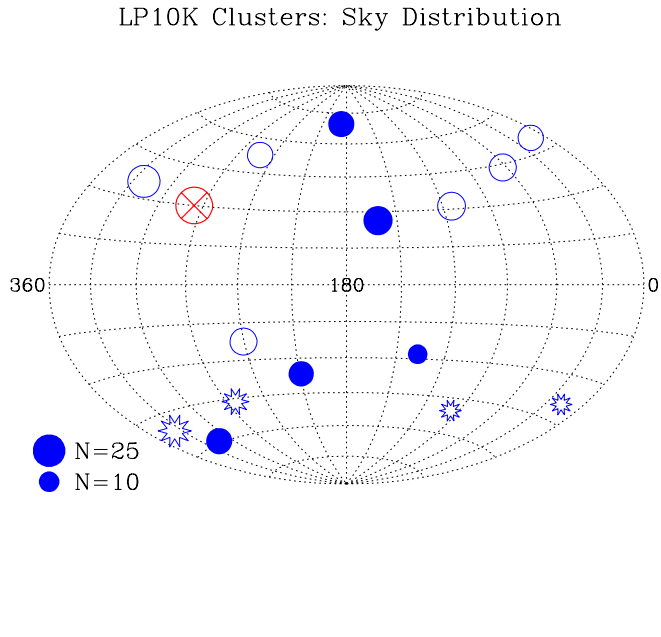


FIG. 1.— Sky positions of the fifteen LP10K clusters. Filled circles represent clusters for which the mean redshift of the LP10K TF sample is $\leq 12,000 \text{ km s}^{-1}$. Open circles represent clusters with mean TF sample redshift $12,000 \text{ km s}^{-1} \leq cz \leq 15,000 \text{ km s}^{-1}$, and starred symbols those with mean $cz > 15,000 \text{ km s}^{-1}$. The number of galaxies in the cluster TF sample is symbolized by the point size, as indicated by the key at the lower left. The “ \times ” enclosed by a circle shows the direction of the LG motion with respect to the CMB.

The prevalence of relatively high-redshift objects in the LP10K TF data set is a consequence of the way sample galaxies were selected, namely, on the basis of magnitude and morphology from CCD images (cf. Paper I), and proximity to the cluster center, not on prior knowledge of the redshift. Most sample galaxies, in fact, did not have a measured redshift prior to the LP10K observations. The high-redshift galaxies—which we define here, somewhat arbitrarily, as those with $cz > 15,000 \text{ km s}^{-1}$ —present a problem only insofar as they reduce the number of objects in the $9000\text{--}12,000 \text{ km s}^{-1}$ redshift shell at which the survey was originally targeted. On the other hand, the presence of higher-redshift galaxies provides some sensitivity to a bulk flow on scales considerably larger than the targeted shell.

To clarify the analysis presented in § 3, it will prove useful to distinguish between the full LP10K TF sample and a subsample that maximizes sensitivity to the originally targeted redshift shell. We construct this subsample by excluding all galaxies with $cz < 7000 \text{ km s}^{-1}$ and $cz > 15,000 \text{ km s}^{-1}$. This cut yields the cluster redshifts and sample sizes given in columns 6 and 8 of Table 1. We henceforward refer to this subsample as the “extended target range” (ETR). The ETR subsample comprises 172

galaxies, most of which are bona fide cluster members, judging from the fairly good agreement between cz_{LIT} and cz_{ETR} given in Table 1. The notable exceptions to this trend are the clusters A3202 and A3381, for which the ETR redshifts are, respectively, $\sim 900 \text{ km s}^{-1}$ greater and $\sim 1300 \text{ km s}^{-1}$ less than the literature values. A3202 is, however, the cluster for which the literature value is the most uncertain, and we are inclined to regard the LP10K ETR redshift as more accurate. For A3381 the source of the discrepancy is probably significant subclustering within the cluster; the LP10K TF sample simply weights a lower-redshift clump more strongly than the studies from the literature.

In summary, it is reasonable to conclude that the ETR subsample is representative of the fifteen LP10K clusters *per se*. This is not to say that all ETR galaxies are members of the virialized cluster cores; indeed, as shown in § 3.2.2, most almost certainly are not, because a Hubble expansion plus bulk flow model turns out to be a much better description of the TF data than a model which assumes all members of a given cluster are equidistant. A second point is that the ETR shell appears to be better described as sampling the redshift range $9000\text{--}13,000 \text{ km s}^{-1}$, as compared with the original upper limit of 12,000.

Distinct from the ETR is the entire LP10K TF data set irrespective of redshift, henceforward the “full sample” (FS). The FS comprises 244 galaxies. Sixty-four of the 72 galaxies not in the ETR have redshifts $> 15,000 \text{ km s}^{-1}$, while the remaining eight have redshifts between 5000 and 7000 km s^{-1} .

3. METHOD

As in Paper I, we use a maximum-likelihood method based on the inverse TF relation, but with two key differences. First, we predict distances from redshift and position on the sky using a Hubble expansion plus bulk flow model. (In Paper I bulk flow was omitted.) The distance in Mpc to the i th galaxy is given by

$$d_i = H_0^{-1} [cz_i - \mathbf{v}_p \cdot \hat{\mathbf{n}}_i], \quad (1)$$

where $\hat{\mathbf{n}}_i$ is a unit vector in the direction of the galaxy, and cz_i its CMB frame redshift in km s^{-1} . (We also consider, and then reject, a model in which cz_i is replaced by the mean redshift of the cluster to which the galaxy nominally belongs; cf. § 4.2 for details.) One or more components of the bulk flow vector \mathbf{v}_p may be treated as free parameters in the maximum likelihood fit, but \mathbf{v}_p is the same for every galaxy in the sample. As in Paper I we take $H_0 = 65 \text{ km s}^{-1} \text{ Mpc}^{-1}$; the adopted value affects only the zero point of the TF relation, not the derived bulk flow vector.

Given d_i , the predicted value of the circular velocity parameter is calculated as

$$\eta_{i,\text{pred}} = -e(m_i - 5 \log d_i - 25 - D) + \alpha \mu_i + \beta c_i \quad (2)$$

where m_i , $\mu_{e,i}$, and c_i are the observed apparent magnitude, effective central surface brightness, and concentration index of galaxy i , respectively (cf. Paper I for details). The quantities D and e are the zero point and slope of the TF relation, while α and β are additional TF parameters whose significance is discussed in Paper I. The other important quantity that enters the likelihood analysis is

TABLE 1
LITERATURE, FULL SAMPLE, AND EXTENDED TARGET RANGE REDSHIFTS^a

Cluster	<i>l</i>	<i>b</i>	<i>cz</i> _{LIT}	<i>cz</i> _{FS}	<i>cz</i> _{ETR}	<i>N</i> _{FS}	<i>N</i> _{ETR}	References ^b
A0260	137.1	-28.1	10621	12046	10505	8	7	4,7
A0496	209.3	-36.6	9831	11215	10124	15	11	4,6,7
A0576	161.3	26.3	11493	11973	11973	20	20	4,6
A1139	251.7	52.7	12265	13491	12310	15	14	2,4
A1228	186.7	69.6	11217	11261	11413	16	13	2,4
A2063	12.7	49.8	10803	12546	10776	14	12	4,6,7
A2199	62.9	43.8	8989	12961	9353	17	12	4,6,7
A2247	114.4	31.2	11472	12881	11360	18	13	4,6,7
A2657	96.7	-50.3	11636	17664	11787	10	3	4,6,7
A2731	313.8	-59.3	9246	11090	9161	16	14	1,5
A3202	263.5	-46.3	11600	16409	12481	17	8	1
A3381	240.4	-22.5	11517	13028	10256	17	12	1,3,5
A3578	321.7	35.8	12269	13074	12840	24	18	1,4
A3733	17.5	-39.5	10791	16257	10903	11	5	5
A3869	336.5	-51.2	11839	19485	12450	26	10	5

Notes: (a) All redshifts are listed as CMB frame radial velocities in km s^{-1} . (b) The entries in the References column are keys to the source(s) of the literature redshift, as follows: (1) Abell, Corwin, & Olowin (1989, ACO). (2) Dale *et al.* 1997; (3) Jorgensen *et al.* 1996. (4) Postman, Huchra, & Geller 1992. (5) Postman & Lauer 1995. (6) Struble & Rood 1991. (7) Wegner *et al.* 1996.

the observed value of the circular velocity parameter, η_i . Recall from Paper I that η_i is defined in terms of an additional TF parameter, f_s , which determines the radius at which the rotation velocity is evaluated from the full RC. This is known as the “ f_s -formulation” of the TF relation (Paper I), and is the approach used here. (An alternative approach discussed in Paper I, the “ x_t -formulation,” is essentially equivalent and is not used in this paper.)

The second key difference from Paper I is that we now properly take into account the statistical effects of having multiple photometric and/or spectroscopic measurements for a large number of individual galaxies. In Paper I we included each photometry/spectroscopy data pair for a particular galaxy as a “data object,” and all such objects entered equally into the likelihood computation. In doing so we neglected the correlations among the various data objects derived from a single galaxy, but crudely estimated their effect by scaling the likelihood statistic by the ratio of distinct galaxies to the total number of data objects. This was a conservative approach, as the actual number of degrees of freedom is greater than the number of distinct galaxies because the repeat measurements are partially independent. Such an approach was acceptable in Paper I because the effects we sought to demonstrate had very strong statistical significance.

The bulk flow parameters, however, have relatively large errors, and it is thus important to employ a rigorous rigorous likelihood statistic. This is done as follows. Suppose that the *i*th distinct galaxy was observed only once spectroscopically, yielding circular velocity parameter η_i , but has n_i photometric measurements (in practice, $n_i \leq 4$), yielding apparent magnitudes m_{ij} , $j = 1, \dots, n_i$. Then the conditional probability density for the observed velocity width, given the n_i photometry measurements and the

redshift is

$$P(\eta_i | m_{ij}, cz_i) = \frac{1}{\sqrt{2\pi\sigma_{\text{eff}}^2}} \exp \left\{ -\frac{[\eta_i - \eta_{i,pred}(\bar{m}_i)]^2}{2\sigma_{\text{eff}}^2} \right\}, \quad (3)$$

where:

1. $\eta_{i,pred}(\bar{m}_i)$ is the predicted circular velocity parameter based on the average of the photometric measurements, $\bar{m}_i = \sum_j m_{ij}$. Because we use a multiparameter TF relation, equation 2, \bar{m}_i symbolizes averages over all relevant photometric quantities, not only apparent magnitude.
2. The observed circular velocity parameter η_i is also derived by combining the spectroscopic measurement with average values of the needed photometric parameters: the inclination i and the effective exponential scale length r_e (cf. Paper I).
3. The effective scatter is computed as the quadrature sum of its four contributions:

$$\sigma_{\text{eff}}^2 = \left(\frac{5e}{\ln 10} \frac{\sigma_v}{d_i} \right)^2 + \sigma_I^2 + \sigma_S^2 + \sigma_P^2/n_i \quad (4)$$

where:

- (a) $\sigma_v = 250 \text{ km s}^{-1}$ is, as in Paper I, the assumed velocity noise relative to the bulk flow model;
- (b) σ_I is the intrinsic scatter in the inverse TF relation, taken as a free parameter in the model;
- (c) σ_S is the portion of the η -error due to spectroscopic measurement errors only. It was modeled as $\sigma_S = \delta v_{\text{rot}}/(v_{\text{TF}} \sin i)$, where δv_{rot} , treated as a free parameter in the model, is the circular

velocity measurement error, assumed constant, and v_{TF} is the predicted value of the circular velocity. The motivation for this error model was discussed in Paper I. (The projection factor $\sin i$ was erroneously neglected in the Paper I analysis.)

(d) σ_P is the rms error in measuring and predicting η due to photometric measurement errors. Thus, it includes the effects of inclination and effective radius measurement errors on the measured η , as well as those of magnitude, surface brightness, and concentration index errors on the predicted η . The various photometric errors were assessed by comparing values for multiply observed objects, and will be described fully in Paper III. In general, σ_P constitutes a very small fraction of the overall error budget.

Note that equation 3 reduces to equation 10 of Paper I when $n_i = 1$.

If galaxy i has two spectroscopic measurements yielding circular velocity parameters η_{i1} and η_{i2} , then another term is present in the likelihood, as follows:

$$P(\eta_{i1}, \eta_{i2} | m_{ij}, cz_i) = \frac{1}{\sqrt{4\pi\sigma_S^2}} \exp \left\{ -\frac{(\eta_{i1} - \eta_{i2})^2}{2(\sqrt{2}\sigma_S)^2} \right\} \times \frac{1}{\sqrt{2\pi\sigma_{\text{eff}}^2}} \exp \left\{ -\frac{[\bar{\eta}_i - \eta_{i,\text{pred}}(\bar{m}_i)]^2}{2\sigma_{\text{eff}}^2} \right\}, \quad (5)$$

where $\bar{\eta}_i = (\eta_{i1} + \eta_{i2})/2$, and the effective scatter is now given by

$$\sigma_{\text{eff}}^2 = \left(\frac{5e}{\ln 10} \frac{\sigma_v}{d_i} \right)^2 + \sigma_I^2 + \sigma_S^2/2 + \sigma_P^2/n_i. \quad (6)$$

Note that the two-spectroscopic measurement likelihood differs from the single measurement case by the presence of a term measuring the probability that the two measurements will differ by the observed amount. The corresponding term for photometric measurement differences does not occur because we are using conditional probabilities of η given m . The presence of this term gives the likelihood analysis greater leverage on the velocity measurement error term δv_{rot} than the Paper I approach, which relied solely on TF residuals to estimate δv_{rot} . In fact, as will be seen, this leads to a $\sim 10\%$ increase in the estimated δv_{rot} , a relatively small change. The better-determined δv_{rot} in turn means that the resultant value of σ_I , the intrinsic TF scatter, is also more reliably determined. Our inclusion of photometric measurement errors, neglected in Paper I, also improves the σ_I estimate. Thus, our present approach affords one of the most accurate estimates to date of the the intrinsic TF scatter, a quantity of considerable interest for galaxy formation theory (e.g., Steinmetz & Navarro 1998).

The overall likelihood for the sample is given by $\mathcal{P} = \prod_i P(\eta_i | m_i, cz_i)$, where the product runs over all distinct galaxies in the sample (as opposed to all data objects as in Paper I), and $P(\eta_i | m_i, cz_i)$ is calculated from equation 3 or equation 5, as appropriate. In practice, likelihood maximization is achieved by minimizing the statistic

$\mathcal{L} = -2 \ln \mathcal{P}$. In all cases, \mathcal{L} is minimized with respect to the various TF parameters (including those characterizing the TF errors), as well as the bulk flow components.

Although the maximum likelihood method is effective for simultaneously determining bulk flow and TF parameters, it does not yield a rigorous measure of goodness of fit (cf. the discussion by Willick *et al.* 1997b). For this purpose, it is useful to define “cluster- χ^2 ” statistic sensitive only to the bulk flow parameters, and changes in which from one model to the next can be used to gauge improvements in the fit. We do so by computing an average radial peculiar velocity v_p and corresponding error δv_p for each cluster, and comparing with the predicted radial peculiar velocity $u = \mathbf{v}_p \cdot \hat{\mathbf{n}}$ from the flow model:

$$\chi_{\text{clust}}^2 = \sum_{i=1}^{15} \left(\frac{v_{p,i} - u_i}{\delta v_{p,i}} \right)^2, \quad (7)$$

where the sum runs over the fifteen LP10K clusters. In calculating the δv_p , we take the scatter contributions σ_I and σ_S to have fixed values, rather than the best-fit values from the maximum likelihood solution. This ensures that χ_{clust}^2 measures only bulk flow errors, not differences in the TF scatter from model to model. The adopted values are $\sigma_I = 0.025$ and $\delta v_{\text{rot}} = 17.5 \text{ km s}^{-1}$, close to the values obtained from the best ETR fit (cf. § 4.4).

4. RESULTS

Before proceeding to the results of the flow analysis, we address two key technical issues: Galactic extinction and the redshift-distance model.

4.1. Burstein-Heiles versus Schlegel-Finkbeiner-Davis extinctions

Two all-sky Galactic extinction maps are presently available: the older Burstein-Heiles (Burstein & Heiles 1978, 1982; BH) maps, which are based on 21 cm column density and faint galaxy counts, and the recently completed Schlegel, Finkbeiner, & Davis (1998; SFD) maps, based on DIRBE/IRAS measurements of diffuse IR emission. The SFD extinctions have been favored in several recent analyses, and indeed were used in Paper I. Unlike BH, the SFD extinctions are based directly on dust emission and have comparatively high spatial resolution. However, it has not been established beyond doubt that they are free of systematic errors, such as could arise from the presence of cold dust invisible to IRAS. The BH extinctions are also vulnerable to possible systematic effects, such as a variable dust-to-gas ratio and galaxy count fluctuations. Thus it seems prudent to use both methods, or linear combinations of them, and see what effect this has on the results.

We have run the likelihood and cluster- χ^2 analyses, for both the ETR and FS samples, correcting apparent magnitudes and surface brightnesses using BH, SFD, and their direct average, (BH+SFD)/2. The results are given in Table 2, of which a full description is given below; here we summarize only the conclusions with regard to extinction. First, the derived flow vector is quite insensitive to which extinction method is used. The flow direction shifts about $+20^\circ$ in longitude and $+10^\circ$ in latitude, and the flow amplitude increases by a few percent, when SFD extinctions

are replaced by BH extinctions. These changes are smaller than the 1σ errors, and thus statistically insignificant. The cluster- χ^2 statistic is also relatively insensitive to the extinction method. For the ETR the SFD extinctions produce a smaller χ^2_{clust} , whereas for the FS the situation is reversed. For both the ETR and the SF, average extinctions, $(\text{BH}+\text{SFD})/2$, yield likelihood and χ^2_{clust} statistics as good, or nearly so, as the better of SFD or BH. We conclude that the flow analysis does not provide clear evidence for the superiority of one extinction scheme over the other, and indicates that averaging them may produce most reliable results overall. We thus adopt the average extinctions to obtain the final flow vectors for the ETR and the FS, as well as to compare with alternative solutions such as flow along the LP94 direction or no flow (see below).

4.2. Distance assignments

The LP10K sample consists, nominally, of cluster galaxies. It is conventional to assume that all members of a given cluster lie at a common distance, regardless of redshift (the “cluster paradigm”). In Paper I, however, we modeled all galaxy distances by the Hubble law, thus assuming that even within a cluster there is a redshift-distance correlation. Such an approach is obviously called for when analyzing the full sample, with its many galaxies well in the background of the targeted clusters. On the other hand, the ETR cluster subsamples have mean redshifts close to published values for the cluster cores, suggesting that the redshift-distance relation for the ETR might be more aptly modeled by the cluster paradigm. However, some previous cluster TF studies have shown that even spirals near cluster cores, as judged by position in redshift space, may exhibit a redshift-distance relation close to pure Hubble expansion (Bernstein *et al.* 1994; Willick *et al.* 1995). The LP10K clusters are too distant, given the large TF errors, to judge which model is better for a given cluster. However, we can address this question by carrying out a cluster paradigm fit to the ETR subsample. To do so we model the distance to the j th galaxy in the i th cluster by

$$d_{ij} = H_0^{-1} [\langle cz_i \rangle - \mathbf{v}_p \cdot \hat{\mathbf{n}}], \quad (8)$$

where $\langle cz_i \rangle$ is the mean redshift of the i th cluster. We take this to be the literature-based redshift, column (4) of Table 1, except in the cases of A3202 and A3381, where we adopt the mean LP10K ETR redshift, column (6) of Table 1 (see the discussion in § 2). This distance model implicitly assumes that any redshift dispersion within a given cluster is due to virial velocities, not to Hubble expansion.

We applied the maximum likelihood algorithm to the LP10K ETR subsample using equation 8 to assign distances, and calculated the resultant χ^2_{clust} . The results are given in row (4) of Table 2. The likelihood statistic is larger, by 11 units, than the best-fit value assuming free expansion. Given that the models have the same numbers of degrees of freedom, this is a highly significant ($\sim 3.3\sigma$) difference. Similarly, χ^2_{clust} is 7.3 units larger for the cluster paradigm fit than for the free expansion fit. These statistics demonstrate that, overall, the redshift-distance relation for the ETR subsample is much better modeled by free expansion than the cluster paradigm.

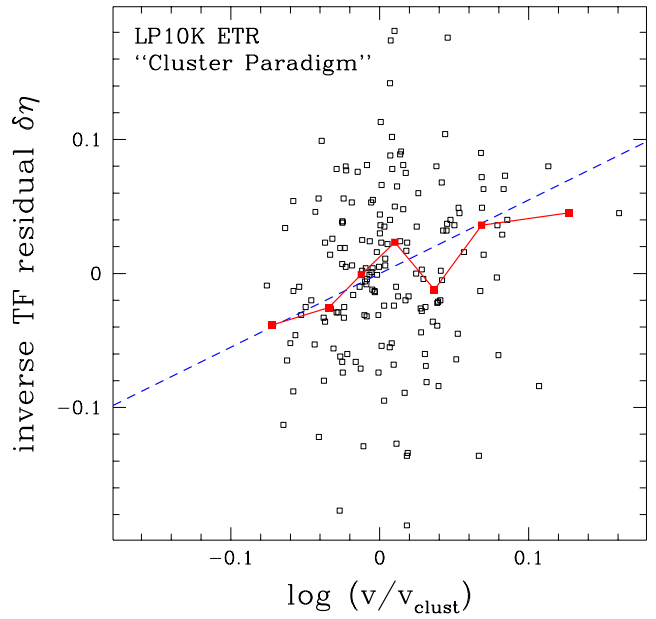


FIG. 2.— Inverse TF residuals from the ETR “cluster paradigm” fit, plotted against $\log(v/v_{\text{clust}})$, where v is the individual galaxy redshift and v_{clust} is the mean redshift of its parent cluster. If the galaxies are better described by free expansion than the cluster paradigm, the residuals are expected to follow the relation $\delta\eta \approx 5e \log(v/v_{\text{clust}})$, shown as the diagonal dashed line in the figure. The connected filled squares show a running median of the residuals, which are seen to follow the expansion relation rather closely. This suggests that the redshift-distance relation for the LP10K TF spirals is, to within the accuracy of the data, close to the free expansion expectation.

This point is demonstrated graphically in Figure 2, where we plot inverse TF residuals from the ETR cluster paradigm fit versus logarithmic redshift differences between a galaxy and its parent cluster. If the cluster paradigm held, there should be no trend. On the other hand, if free expansion is a better model, galaxies with redshifts smaller than the cluster mean are closer than those with redshifts larger than the cluster mean. This distance correlation translates into a trend of TF residuals with relative redshift given by $\delta\eta \approx 5e \log(v/v_{\text{clust}})$, where $e \approx 0.12$ is the inverse TF slope. This expected trend is indicated as a dashed line in Figure 2. The trend in the individual residuals is difficult to discern by eye because of the large TF scatter. However, a running median of the residuals, shown as connected solid squares, closely follows the residual trend. This confirms that the large improvement in the fit when the cluster paradigm is abandoned does in fact derive from expansion motions of sample galaxies. Like the samples of Bernstein *et al.* (1994) and Willick *et al.* (1995), TF cluster samples in the LP10K ETR appear to be clusters in name only; dynamically they more closely approximate field galaxies.

Thus, for the remainder of this paper we assume that the Hubble expansion plus bulk flow model, equation 1, is the most accurate representation of the redshift-distance relation for the LP10K galaxies. We note, however, that the bulk flow derived from the cluster paradigm fit, line

4 in Table 2, differs by less than 1σ in amplitude and direction from the bulk flow derived with the expansion model.

4.3. Main results

The main results obtained from the maximum-likelihood fits are presented in Table 2. The bulk flow parameters are expressed in terms of amplitude and direction in columns 1–3. The amplitudes have *not* been corrected for the bias discussed in § 5. The directions are unbiased, however (§ 5). Columns (4) and (5) list the likelihood and χ^2_{clust} statistics defined in § 3. Column (6) gives the extinction method used in each fit; for reasons discussed in § 4.1, we now focus only on fits using the mean extinctions, $(\text{BH+SFD})/2$. Column (7) provides keys to details of the fits given in the table notes.

Our final bulk flow vectors are obtained from the likelihood fits in which all three components of the flow velocity were varied, namely, the first lines in the ETR and FS sections of the table. The flow amplitudes, 961 km s^{-1} for the ETR and 873 km s^{-1} for the FS, are biased high by 33% and 25% respectively, as determined from the Monte Carlo analysis of § 5. When corrected for these biases, they yield the flow amplitudes quoted in the Abstract and Summary, § 6.3. The cluster- χ^2 statistic does not necessarily take on its minimum value for these fits, because the flow parameters are computed by maximizing likelihood, not by minimizing χ^2_{clust} . However, the maximum-likelihood fits produce values of χ^2_{clust} within ~ 1 unit of its minimum value.

Other entries in Table 2 test alternative flow directions. The lines in which the direction is given as $l = 276^\circ$, $b = 30^\circ$ give results of fits in which the flow was assumed a priori to be parallel to the LG peculiar velocity, and only the amplitude was varied. The likelihood statistics for these fits differ very little from the best-fit values. Indeed, this choice of flow direction produces a smaller χ^2_{clust} than does the best fit for the ETR. The LP10K bulk flow may thus be described, to better than 1σ accuracy, as being in the same direction as the LG motion.

The lines in Table 2 in which the direction is given as $l = 343^\circ$, $b = 52^\circ$ give results of fits in which the flow was assumed a priori to be parallel to the LP94 bulk flow. The best-fit flow amplitudes along this axis are much smaller, for both the ETR and FS, than the 700 km s^{-1} reported by LP94. Moreover, the likelihood and χ^2_{clust} values for this fit indicates that these solutions are poor models in comparison with that in which the flow is held parallel to the LG motion. As these two models have the same number of free parameters, these differences are highly significant. In short, the LP10K data set is inconsistent with the LP94 bulk flow.

Table 2 also lists the fit results when $V_B \equiv 0$, i.e., pure Hubble flow in the CMB frame. This yields the lowest likelihood and largest χ^2_{clust} values of all fits considered (except the cluster paradigm fit discussed in § 4.2). We defer to § 5 a quantitative discussion of the confidence level with which the data set enables us to rule out the $V_B \equiv 0$ model. However, from the change in the cluster- χ^2 statistic between the no-flow model and the best-fit model for the FS, $\Delta\chi^2_{\text{clust}} = 8.78$ with the addition of three degrees of freedom, we can estimate that the $V_B \equiv 0$ model is ruled out at about the 2.4σ level. Our Monte-Carlo assessment

of significance levels (§ 5) roughly confirm this estimate.

In Figures 3 and 4 we plot CMB frame radial peculiar velocities of the 15 LP10K clusters, for the ETR and FS samples respectively. The velocities plotted are those that went into the χ^2_{clust} calculations for the $V_B = 0$ model. They are derived from the mean inverse TF residuals for each cluster, assuming that all cluster galaxies lie at the mean cluster velocity. (In the case of the FS, this is not always a good assumption, but it is the only way to assign a peculiar velocity to a given cluster.) The point sizes are inversely proportional to peculiar velocity errors, so that large symbols carry proportionally more weight in determining the bulk flow solution. In each figure error bars are drawn for two points to calibrate the size-error mapping. In Figure 3, the velocities are plotted against the cosine of the angle between the cluster and the CMB dipole direction ($l = 276^\circ$, $b = 30^\circ$), the flow direction which yielded the smallest χ^2_{clust} among the ETR fits. In Figure 4, the velocities are plotted against the cosine of the angle between the cluster and $l = 272^\circ$, $b = 10^\circ$, the flow direction which yielded the smallest χ^2_{clust} for the FS. The tilted solid lines in each figure represent the predicted radial peculiar velocities from the respective flow models.

Figures 3 and 4 provide visual evidence of the bulk flow solutions found from the likelihood analysis. In each case, the clusters near the apex of the flow axis have peculiar velocities which are positive in the mean; clusters nearer the antapex tend to have negative velocities. The notable exceptions to the trend are the clusters A2657 and A260, which lie near the antapex of the flow and have velocities $\gtrsim 0$. However, as indicated on the figures, these clusters have comparatively few members. A2657 is in consistent at the $< 1\sigma$ level with the flow model for the ETR, and A260 is consistent with the flow model for the FS. Thus, although these clusters deviate from the trend, the deviation is not statistically significant. For the FS, the cluster A2247 is a large ($\sim 2\sigma$) outlier from the flow model, but in a sense which reinforces the flow.

While Figures 3 and 4 show why the data favor a large bulk flow in the general direction of the CMB dipole, they also reflect the relatively large scatter in the TF relation. At the distances of the LP10K clusters, even samples of 10–20 TF galaxies give rise to 1σ peculiar velocity errors approaching 1000 km s^{-1} . As a result, there is considerable scatter about the mean trend in the diagrams, and the flow solutions themselves have significant errors.

TABLE 2
MAXIMUM LIKELIHOOD FIT RESULTS

$V_B^{(1)}$	l	b	\mathcal{L}	χ^2_{clust}	Extinctions	Notes
Results for ETR:						
961	266	19	-892.6	12.21	(BH+SFD)/2	2,4
994	275	25	-891.5	13.94	BH	2,4
970	252	12	-891.8	12.04	SFD	2,4
805	252	18	-881.6	19.48	(BH+SFD)/2	3,4
916	276	30	-892.0	11.60	(BH+SFD)/2	2,5
202	343	52	-888.3	16.63	(BH+SFD)/2	2,6
0	-	-	-888.0	17.92	(BH+SFD)/2	2,7
Results for FS:						
873	272	10	-1226.2	16.94	(BH+SFD)/2	2,4
896	285	14	-1226.5	15.84	BH	2,4
838	259	0	-1223.5	20.17	SFD	2,4
766	276	30	-1226.1	17.79	(BH+SFD)/2	2,5
151	343	52	-1221.7	24.81	(BH+SFD)/2	2,6
0	-	-	-1221.4	25.72	(BH+SFD)/2	2,7

Notes: (1) Best fit bulk flow amplitude, in km s^{-1} . This value has *not* been corrected for the statistical bias effect discussed in § 4, and thus is $\sim 25\text{--}30\%$ larger than the values quoted in the abstract, which have been corrected. (2) Expansion model used for redshift-distance relation (see text for details). (3) “Cluster paradigm” model used for redshift-distance relation (see text for details). (4) All three Cartesian components of bulk flow vector varied in fit. (5) Bulk flow amplitude varied (negative values allowed), but direction fixed along CMB axis, $l = 276^\circ$, $b = 30^\circ$. (6) Bulk flow amplitude varied (negative values allowed), but direction fixed along LP94 flow axis, $l = 343^\circ$, $b = 52^\circ$. (7) Pure Hubble flow ($V_B \equiv 0$) assumed.

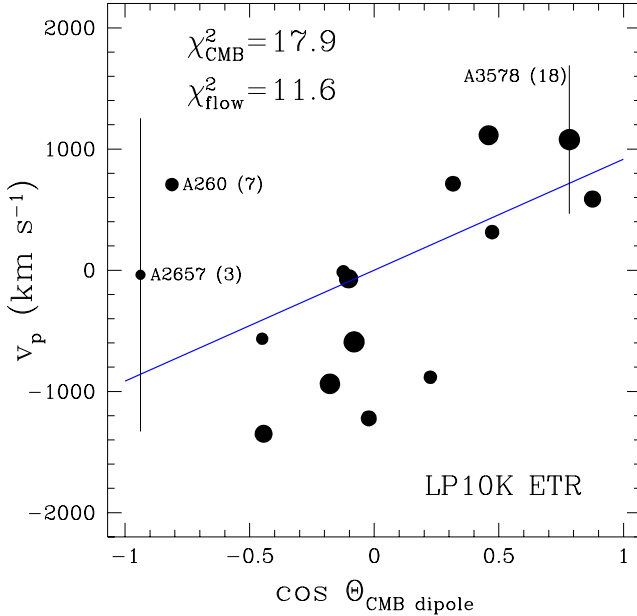


FIG. 3.— CMB frame peculiar velocities of the 15 LP10K clusters, plotted against the cosine of the angle between the cluster position on the sky and the apex of the CMB dipole, $l = 276^\circ$, $b = 30^\circ$. The cluster TF samples are restricted to the ETR. Point sizes are inversely proportional to the peculiar velocity errors. The largest (A2657) and smallest (A3578) of these errors are shown as error bars, with the number of ETR galaxies in those clusters also indicated. The cluster which deviates most significantly from the bulk flow fit, A260, is also labeled. The tilted line shows the best-fit bulk flow amplitude, 916 km s^{-1} , when the when the bulk flow direction is fixed toward the CMB dipole. See text for further details.

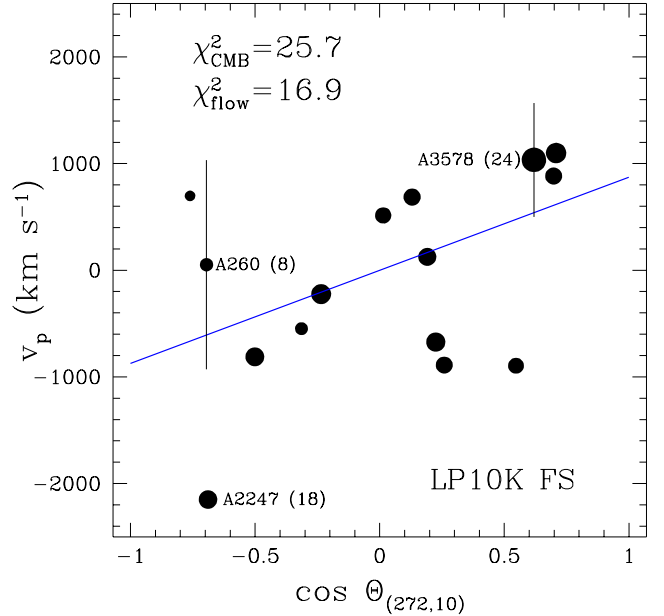


FIG. 4.— Same as the previous figure, except cluster peculiar velocities for the LP10K *full sample* are plotted now against the cosine of the angle between the cluster position on the sky and best-fit flow direction for the FS, $l = 272^\circ$, $b = 10^\circ$. Peculiar velocity error bars are indicated for A3578 and A260. Also identified is A2247, the only 2σ outlier from the fit.

4.4. TF parameters

In Paper I we applied a pure Hubble flow model to the LP10K full sample in order to study the properties of the TF relation. Here we have shown that the addition of a bulk flow to the redshift-distance model significantly improves the fit likelihood. It is thus worth asking whether the TF parameters themselves have changed significantly. The TF parameters derived from the best-fit ETR and FS flow models are listed in Table 3. The meaning of the parameters given in the table was described briefly in § 3, and in greater detail in Paper I.

Table 3 should be compared with Table 2 (line 4) of Paper I, which lists the same parameters from the Hubble flow fit of that paper. The parameters are seen to have changed very little as a result of the flow model and the adoption of a more rigorous likelihood algorithm. In particular, the values of α , which measures the surface-brightness dependence of the TF relation, and of f_s , the number of disk scale lengths at which the rotation curve should be evaluated to optimize the TF relation, and to which particular physical significance was ascribed in Paper I, are seen to be virtually unchanged. The TF slope and zero point have changed very slightly as a result of adopting the flow model.

A somewhat more significant change is seen in the value of the rotation velocity measurement error δv_{rot} (called δv_{TF} in Paper I), which has increased by about 10%. This change may be ascribed, as discussed in § 3, to the proper accounting for repeat spectroscopic measurements and photometric errors in the improved likelihood method of this paper. As a result, δv_{rot} is more accurately determined. This, in turn, means that the intrinsic TF scatter is better constrained than in Paper I. The value of σ_I for the FS, 0.030, is the more reliable because of the larger sample size. The Monte-Carlo simulations enable us to test for biases in the TF parameters just as the bulk flow parameters, and they show that the maximum likelihood value of σ_I is biased low by about 10%. They also show that the rms error in the determination of σ_I is about 25%. Taking these into account, our best estimate of the inverse TF scatter is $\sigma_I = 0.033 \pm 0.008$ dex. The corresponding value of the forward TF scatter is $\sigma_{I,forw} = \sigma_I/e = 0.28 \pm 0.07$ mag.

5. MONTE-CARLO SIMULATIONS

5.1. Details of the simulations

The true sky positions, redshifts, apparent magnitudes, and inclinations of all LP10K TF galaxies were used as initial input to the simulations. Distances were assigned to each galaxy according to a bulk flow model, $d = H_0^{-1}[cz - \mathbf{v}_p \cdot \hat{\mathbf{n}}]$. Absolute magnitudes, $M = m - 5 \log(d) - 25$, where thus derived, and a preliminary circular velocity parameter $\eta_0 = -e(M - D)$ was assigned to each galaxy. The TF parameters were taken to be $e = 0.12$ and $D = -21.62$, similar to the observed values. The surface-brightness and concentration-index dependences of the TF relation were neglected in the simulations.

A Gaussian random variable of mean zero and dispersion $\sigma_I = 0.032$ was added to η_0 , yielding a “true” circular velocity parameter η_1 and a corresponding projected rotation velocity $v_{rot}^{proj} = 158.1 \sin i \times 10^{\eta_1} \text{ km s}^{-1}$, where i was the observed galaxy inclination. A second Gaussian random variable of dispersion 16 km s^{-1} was added to v_{rot}^{proj} to simulate the effect of spectroscopic measurement errors. If there were two spectroscopic observations of an individual galaxy, independent random errors were added to each. The scattered rotation velocities were then divided by $\sin i$ to produce the final observational values of v_{rot} and η . Finally, Hubble flow noise was simulated by scattering each redshift by a Gaussian random variable of dispersion $\sigma_v = 250 \text{ km s}^{-1}$.

The above procedure yields a simulated data set that mimics in most respects the statistical properties of the real one. Photometric errors were not included in the simulations, but these have a negligible effect on the overall TF scatter. The simulated data sets were then subjected to the same cuts on absolute magnitude, inclination, etc. (cf. Paper I) as the real one. Consequently, the results of applying the maximum likelihood code to them should faithfully reflect the random errors in the recovered peculiar velocity vector.

5.2. Choice of simulated bulk flow vectors

Ideally one would like to simulate a suite of universes with a large variety of underlying bulk flow vectors. One could then ask, for any given flow vector, what is the probability of obtaining the result found from the real data? One could then invert this relation using Bayesian statistics and obtain the probability distribution of the true vector given the observed data. However, because of the relatively large observational errors for LP10K, it is not essential to carry out this full-blown analysis here. For our present purposes, two types of simulations, each corresponding to a reasonable “paradigm,” suffice:

1. Paradigm I. The Hubble flow beyond $\sim 10,000 \text{ km s}^{-1}$ is isotropic in the CMB frame, i.e., $V_B = 0$. The only perturbation to Hubble expansion are random velocities.
2. Paradigm II. The motion of the Local Group relative to the CMB is generated on very large scales, $\gtrsim 300h^{-1} \text{ Mpc}$. The bulk flow of the LP10K sample would then be similar to the peculiar velocity of the Local Group. For these simulations we adopt $V_B = 625 \text{ km s}^{-1}$ toward $l = 270^\circ$, $b = 30^\circ$. The random velocities are, of course, still present.

5.3. Results of simulations

Four Monte-Carlo runs were carried out in total, two based on paradigm I and two on paradigm II. For each paradigm the FS and ETR samples were simulated. Each of the four runs consisted of 10^4 simulated data sets and likelihood analyses. The results of each simulation were a recovered bulk flow components V_x , V_y , and V_z , as well as the various TF parameters and likelihoods.

TABLE 3
TULLY-FISHER PARAMETERS

D	e	α	β	f_s	σ_I	δv_{rot}	FS/ETR
-21.664	0.1138	0.0485	0.0427	1.993	0.0227	17.5	ETR
-21.675	0.1170	0.0500	0.0407	2.029	0.0302	17.7	FS

Notes: TF parameters obtained from the best-fit maximum likelihood flow solutions in Table 2, for both the ETR and the FS. The meaning of the various parameters is given in § 3. The quantity δv_{rot} is expressed in km s^{-1} .

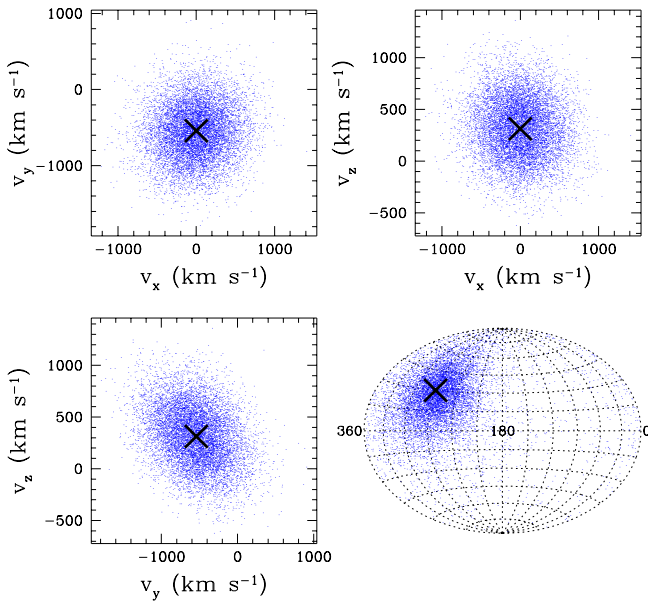


FIG. 5.— Ten thousand random realizations of the LP10K full sample in a universe in which the true bulk flow is 625 km s^{-1} towards $l = 270^\circ$, $b = 30^\circ$. The recovered Galactic Cartesian velocity components are plotted in the upper panels and the lower left panel; the lower right panel shows the recovered direction of the flow in Galactic coordinates.

Figure 5 shows the results of simulating the LP10K full sample based on paradigm II. (The plot that results from simulations of the ETR subsample is quite similar in appearance.) Several key features of the plot may be noted. First, the recovered individual velocity components are very nearly unbiased. The input components of the bulk flow are $V_x = 0$, $V_y = -541.3$, and $V_z = 312.5 \text{ km s}^{-1}$. The corresponding mean recovered values are $\langle V_x \rangle = -7.8 \pm 3.2$, $\langle V_y \rangle = -554.0 \pm 3.5$, and $\langle V_z \rangle = 318 \pm 2.8 \text{ km s}^{-1}$. Thus, the individual components are only very slightly ($\lesssim 15 \text{ km s}^{-1}$) biased. This bias is very small in comparison with the rms scatter in the derived components, which is $\sim 300 \text{ km s}^{-1}$. The accuracy of the components similarly translates into a mean flow direction toward $l = 270.3^\circ$, $b = 30.1^\circ$, virtually identical to the input direction. The rms error in the flow direction about the mean is 35° . Thus, the simulations demonstrate that the LP10K can recover the direction of the bulk flow, and the value of its individual Cartesian components, in

an unbiased fashion. The residual biases are so small in comparison with the scatter of a single measurement that they may be neglected.

The amplitude of the recovered flow vector is, on the other hand, biased high. This occurs because the scatter in the individual components can only increase their quadrature sum. To quantify this bias we take the average of all 10^4 recovered velocity amplitudes, which we find to be 784 km s^{-1} , or 25.4% higher than the input value of 625 km s^{-1} . We take this as a measure of the velocity amplitude bias for the LP10K FS. For the ETR, the bias is somewhat larger, 33.1%. Thus, the final quoted values for the bulk flow derived from the FS and ETR samples are corrected by factors $(1.254)^{-1}$ and $(1.331)^{-1}$, respectively, relative to the values which appear in Table 2.

We calculate the error in the recovered bulk flow amplitude as the average over 10^4 simulations of $|V_B - \langle V_B \rangle|$. For FS, this yields $\Delta V = 250 \text{ km s}^{-1}$. For the ETR the same procedure yields $\Delta V = 280 \text{ km s}^{-1}$. These are the estimates of the 1σ bulk flow amplitude errors given in the abstract.

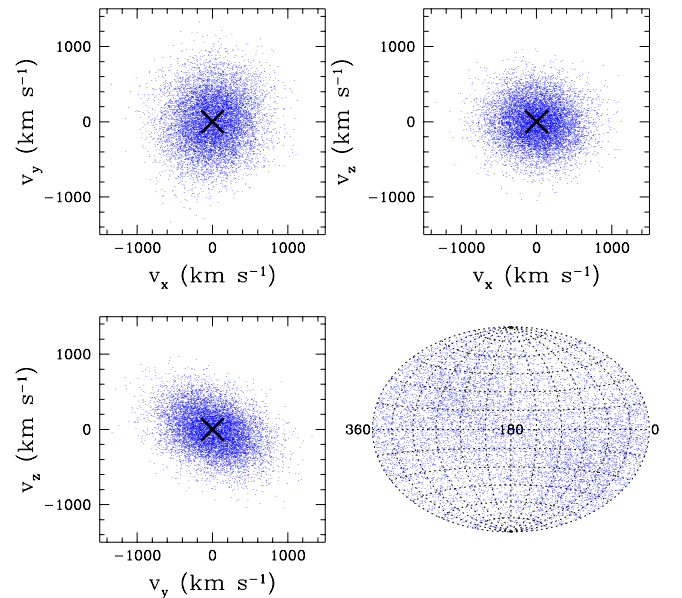


FIG. 6.— Ten thousand random realizations of the full LP10K sample in a universe with zero bulk flow in the CMB frame. The quantities plotted are the same as in the previous figure.

The paradigm II simulation enabled us to estimate biases and errors under the assumption that the detected ETR and FS flows are real. In order to measure how well the LP10K data set rules out the hypothesis of convergence, however, we need to consider the paradigm I simulation, in which the true bulk flow vanishes in the CMB frame. The results of 10^4 paradigm I simulations of the LP10K FS sample are shown in Figure 6. As before, heavy crosses mark the true values of the Cartesian components of the flow, in this case, $V_x = V_y = V_z = 0$. The average values recovered from the simulations are $V_x = 3.8 \pm 3.2 \text{ km s}^{-1}$, $V_y = 5.2 \pm 3.5 \text{ km s}^{-1}$, $V_z = -12.6 \pm 2.7 \text{ km s}^{-1}$. Thus, the likelihood analysis again recovers, on average, the true flow components with negligible bias. The lower right panel of Figure 6 demonstrates that there is no preferred direction for the recovered velocity vector. The points are well-distributed around the sky, although a slight preference for the CMB apex and antapex quadrants is apparent. (This tendency is also manifested in the non-circular shape of the V_y versus V_z plot.) This represents a small geometrical bias that results from the imperfect isotropy of the LP10K clusters.

To determine the confidence level at which we can rule out convergence, we proceed as follows. We ask the question, what fraction of paradigm I simulations yield derived flow vectors of amplitude $V_B \geq fV_{data}$, and in a direction $\hat{\mathbf{n}}$ such that $\hat{\mathbf{n}} \cdot \hat{\mathbf{n}}_{data} \geq \cos \theta_{RMS}$, where θ_{RMS} is the 1σ directional error of the flow, and V_{data} and $\hat{\mathbf{n}}_{data}$ are the derived amplitude and direction of the LP10K observed (ETR and FS) flows. We choose the parameter f such that *half* of all paradigm II simulations satisfy these threshold criteria, with V_{data} and $\hat{\mathbf{n}}_{data}$ are replaced by the mean paradigm II amplitude and direction; this yields $f \approx 0.8$. In other words, we ask, “What fraction of zero-flow simulations produce flow results that occur half the time when the flow is real?” The answer to this question gives the probability that the LP10K results occur by chance in a $V_B = 0$ universe.

When we carry out this exercise, we find that 5.3% (525/10000) of all ETR paradigm I simulations, and 2.9% (290/10000) of the FS paradigm I simulations, meet these criteria. We thus deduce that we can rule out the hypothesis that the Hubble flow has converged to the CMB frame at distances less than $\sim 100h^{-1}$ Mpc at the 94.7% confidence level from the ETR subsample. Using the full LP10K TF sample, we can rule out the convergence hypothesis at the 97.1% confidence level. These significance levels are roughly consistent with those we deduced in § 4.3 from changes in the χ^2_{clust} statistic between the no-flow and best-fit models in Table 2.

6. FURTHER DISCUSSION AND SUMMARY

The results presented in this paper suggest that the volume of the local universe within $\sim 15,000 \text{ km s}^{-1}$ of the LG possesses a bulk peculiar velocity of $\sim 450\text{--}950 \text{ km s}^{-1}$ with respect to the CMB frame. In this section, we discuss the significance of this finding.

6.1. How reliable are the results?

first, we must ask, is the LP10K bulk flow real? There are several reasons for caution. The statistical significance level is not high, somewhat greater than 2σ . A result at such a modest significance level must be confirmed with

independent data sets. We reiterate that the LP10K survey includes elliptical galaxy FP data in the same fifteen clusters. In several years the observations and reduction of the elliptical sample will be completed, and will provide an independent check of the flow measured from spiral galaxies using the TF relation.

There are other recent flow analyses to compare with the present result. The most encouraging comparison is with the recently completed SMAC survey of Hudson *et al.* (1998a,b). The SMAC sample is about 75% as deep as LP10K, but has similarly good sky coverage, and involves many more galaxy clusters and individual galaxies. Moreover, SMAC is an FP survey of elliptical galaxies, and thus is completely independent from the LP10K TF data. It is thus noteworthy that the bulk flow vectors obtained from the two programs are in good agreement in both amplitude and direction (cf. §1). The two results together constitute a strong argument for the reality of the flow.

The LP10K and SMAC findings are, however, at variance with the results of the SFI/SCI survey of Giovanelli and coworkers (Giovanelli *et al.* 1998a,b; Dale *et al.* 1998). SFI/SCI is an I -band TF survey comprising numerous cluster and field galaxies. Its depth is somewhat less than LP10K’s, but quite similar to SMAC’s, at $8000\text{--}10,000 \text{ km s}^{-1}$. The most consistent result from SFI/SCI is the clear signal of convergence of the Hubble flow to the CMB frame by a distance of 6000 km s^{-1} . At $10,000 \text{ km s}^{-1}$, the SFI/SCI group finds the bulk flow to be $\leq 200 \text{ km s}^{-1}$ with high confidence, and to be consistent with zero (Dale *et al.* 1998).

There is no simple way at present to resolve the discrepancy between the LP10K and SMAC results, on the one hand, and those of the SFI/SCI project, on the other. What will be required is a systematic comparative analysis of the data sets on a cluster by cluster, and object by object, basis. Such a comparison will be possible when all three groups have published their complete data sets. This will occur in the near future for the LP10K TF sample in Paper III of this series.

6.2. Interpretation

The discussion above shows that the evidence for a $\gtrsim 600 \text{ km s}^{-1}$ bulk flow on a $\gtrsim 150h^{-1}$ Mpc scale is suggestive but not yet compelling. Bearing this in mind, let us for the moment take the LP10K and SMAC results at face value and ask, what are the implications for cosmology? Peculiar velocities arise naturally within the gravitational instability scenario for structure formation. The amplitude and coherence scale of bulk flows thus reflect both the power spectrum of density fluctuations and the value of the density parameter Ω_M , and can, in principle, provide constraints on these important cosmological quantities.

More specifically, consider the mean square amplitude of the bulk velocity on a scale R . According to linear gravitational instability theory it is given by (e.g., Strauss & Willick 1995)

$$\langle v^2(R) \rangle = \frac{H_0^2 \Omega_M^{1.2}}{2\pi^2} \int_0^\infty P(k) \widetilde{W}^2(kR) dk, \quad (9)$$

where Ω_M is the present value of the matter density parameter, $P(k)$ is the mass fluctuation power spectrum, and

$\widetilde{W}(kR)$ is the Fourier transform of the window function of the sample, $W(r)$. Precise determination of the window function is notoriously difficult for real samples. A common approximation, the “tophat” window function, clearly does not apply to the LP10K sample, which attempted to sample a shell rather than a full spherical volume. When restricted to the extended target range, LP10K does indeed approximate a shell, with selection probability roughly constant for between $R_1 = 90h^{-1}$ Mpc and $R_2 = 130h^{-1}$ Mpc. A reasonable representation for the ETR window function is thus

$$W_{\text{ETR}}(r) = \frac{3}{4\pi(R_2^3 - R_1^3)} \times \begin{cases} 1, & R_1 \leq r \leq R_2; \\ 0 & \text{otherwise.} \end{cases} \quad (10)$$

The corresponding window function in Fourier space is

$$\widetilde{W}_{\text{ETR}}(x_1, x_2) = \frac{3}{f^3 - 1} \left[f^3 \frac{j_1(x_2)}{x_2} - \frac{j_1(x_1)}{x_1} \right], \quad (11)$$

where $x_1 = kR_1$, $x_2 = kR_2$, $f = R_2/R_1$, and $j_1(x)$ is the first spherical Bessel function. (The reader may note that this form of the window function tends to the usual tophat form in the limit $R_2 \gg R_1$.) Substitution of equation 11 into equation 9 yields, for an adopted cosmology and power spectrum, the mean square amplitude of the bulk flow for the LP10K ETR subsample.

Before making this calculation, a related issue should be clarified.⁴ The value of $\langle v^2 \rangle$ in a given window is three times the mean square value of any individual Cartesian velocity component. Consequently, the velocity amplitude has a Maxwellian distribution, $P(v)dv \propto v^2 \exp(-3v^2/2\langle v^2 \rangle)$. The significance of the observed velocity must be gauged relative to this distribution. In particular, one may choose a significance level F , say, and a corresponding velocity amplitude v_F , such that $P(v \geq v_F) = 1 - F$. A brief calculation then shows that

$$v_F = \sqrt{\frac{2}{3}} V_{\text{RMS}} y_F, \quad (12)$$

where $V_{\text{RMS}} = \sqrt{\langle v^2 \rangle}$, and y_F is the solution to the equation

$$F = \text{erf}(y_F) - \frac{2y_F}{\sqrt{\pi}} e^{-y_F^2}. \quad (13)$$

With this procedure we find, for example, that 1% of volumes will exhibit $v \geq 1.945 V_{\text{RMS}}$ ($F = 0.99$), while 0.1% will exhibit $v \geq 2.329 V_{\text{RMS}}$ ($F = 0.999$). (This calculation refers only to cosmic variance, and neglects observational error.)

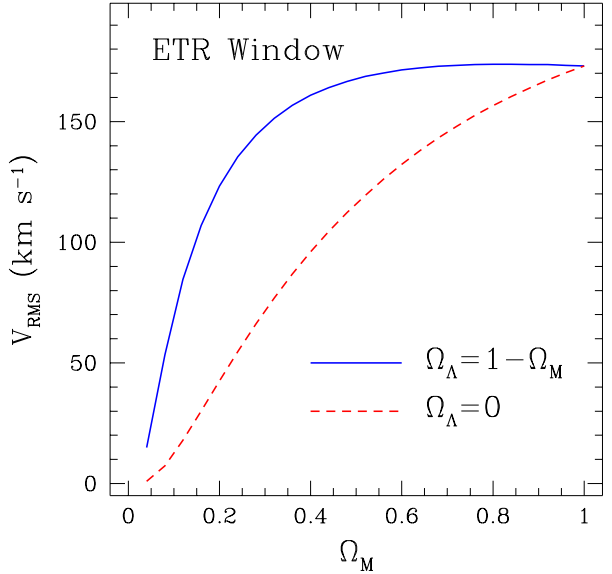


FIG. 7.— The predicted RMS velocity for a shell of inner radius $90h^{-1}$ Mpc and $130h^{-1}$ Mpc, the volume probed by the LP10K ETR subsample. Scale-invariant, COBE-normalized power spectra are used in the calculations. The solid line shows predictions for a spatially flat universe, the dashed line for a $\Lambda = 0$ universe.

Figure 7 shows the results of calculating V_{RMS} through the LP10K ETR window, for $0 < \Omega_M \leq 1$ and COBE-normalized CDM-type power spectra. A Hubble constant of $65 \text{ km s}^{-1} \text{ Mpc}^{-1}$ and a baryon abundance $\Omega_b h^2 = 0.025$ were adopted for the calculation. It is evident that V_{RMS} is quite small in comparison with the measured value of 720 km s^{-1} for the LP10K ETR. If, for example, we consider cosmological parameters favored by recent measurements of Type Ia Supernovae, $\Omega_M = 0.3$, $\Omega_\Lambda = 0.7$ (Riess *et al.* 1998; Perlmutter *et al.* 1999), $V_{\text{RMS}} = 150 \text{ km s}^{-1}$. Thus, 99% of ETR volumes in the universe should exhibit bulk flows less than 292 km s^{-1} in such a universe, and 99.9% of such volumes should possess bulk flows less than 349 km s^{-1} . The corresponding values for $\Omega_M \approx 1$ are only about 17% larger. For low-density, open universes V_{RMS} is several times smaller than for a flat universe of the same Ω_M .

We have also shown that the LP10K full sample, more than 25% of whose members have $0.05 < z \leq 0.1$ and thus lie well beyond the ETR window, yields as strong a signal of large-scale bulk flow as the ETR. It is more difficult to calculate expected theoretical values for the FS, because its window function is poorly defined. However, we gain insight into the effect of the added depth by crudely approximating the FS window function as having the same form as the ETR’s, equation 10, but with $R_2 = 180h^{-1}$ Mpc. (We leave the lower limit at $90h^{-1}$ Mpc, as there are only 8 FS galaxies in the foreground of the ETR.) When V_{RMS} is calculated for this window function, one finds it to be $\sim 20\text{--}30\%$ smaller, for given values of Ω_M and Ω_Λ , than it was for the ETR window. Thus, the FS bulk flow of

⁴The author is indebted to Paul Steinhardt for insightful comments on which the following discussion is based.

700 km s⁻¹, taken at value, exceeds theoretical predictions by a larger margin than the ETR result.

A more thorough exploration of parameter space could, of course, yield slightly larger values of V_{RMS} . This is not necessary here, because the errors on the LP10K flow amplitudes are too large to strongly rule out models at present. The important point is simply that bulk flows on $\gtrsim 100h^{-1}$ Mpc scales are well-suited as probes of large-scale power. In particular, the results of this paper, if ultimately proven correct, would indicate the need for models with more power on large scales than COBE-normalized CDM models can provide. A similar conclusion was reached for the LP94 bulk flow by Strauss *et al.* (1995).

We can anticipate future data sets that will probe bulk streaming on scales $\gtrsim 300h^{-1}$ Mpc. Such measurements will not be possible with methods such as TF and FP, for which peculiar velocity errors become prohibitively large at $z \gtrsim 0.1$. Type 1a supernovae (e.g., Riess *et al.* 1997) are sufficiently accurate distance indicators for this purpose, although it may prove difficult to assemble the required full-sky samples. Perhaps the most promising approach is measurement of the Sunyaev-Zel'dovich (SZ) effect in rich clusters. When combined with X-ray data, SZ measurements yield peculiar velocity estimates with an accuracy of 500–1000 km s⁻¹ (Holzapfel *et al.* 1997). Moreover, SZ measurement errors, although relatively large, do not increase with distance (in contrast to those of methods such as TF, FP and SN Ia), and thus provide a unique probe of bulk flows on scales $z \gtrsim 0.1$.

It is notable that the LP10K and SMAC flow vectors are within $\sim 30^\circ$ of the CMB dipole. If one subtracts the LG velocity from these vectors, little or no motion is left. Should the same pattern hold on much larger scales, one might legitimately question the special character we assign the CMB frame of reference in analyzing the Hubble expansion. Of course, to do so would also require a non-kinematic explanation of the $\Delta T/T \sim 10^{-3}$ dipole anisotropy which is consistent with the fact that higher-order anisotropies are two orders of magnitude smaller. Such scenarios have been proposed in the past (e.g., Paczynski & Piran 1990), but they require substantial modifications of standard Big Bang cosmology. The present data do not compel us to seriously consider such alternatives, but it is worth bearing in mind that future data could push us in that direction.

6.3. Summary

We have used the LP10K TF sample to measure the bulk peculiar velocity on a $\gtrsim 150h^{-1}$ Mpc scale. Both the full sample of 244 galaxies, and a subsample restricted to galaxies with $7000 \leq cz \leq 15,000$ km s⁻¹, the “extended target range” or ETR, were considered. The derived bulk flow was the same, within the errors, for both samples: $v_B = 720 \pm 280$ km s⁻¹ toward $l = 266^\circ$, $b = 19^\circ$ for the ETR, and $v_B = 700 \pm 250$ km s⁻¹ toward $l = 272^\circ$, $b = 10^\circ$ for the full sample. The overall 1σ directional uncertainty is $\sim 35^\circ$. These results were obtained using a maximum likelihood algorithm that minimizes selection and Malmquist biases. Residual biases, which have to do with the geometry of the sample and the fact that Cartesian velocity component errors add in quadrature, were calibrated using Monte-Carlo simulations. These showed

that the raw maximum-likelihood flow amplitude is biased high by $\sim 25\%$. The results quoted above are corrected for this bias. The simulations also enabled us to estimate that the probability the survey would yield the derived flow vectors by chance, if in reality the Hubble flow has converged to the CMB frame at distances $\lesssim 100h^{-1}$ Mpc, is 5.3% for the ETR and 2.9% for the full sample.

The LP10K flow is similar in amplitude and scale to the bulk motion found by Lauer & Postman (1994) from their analysis of 119 brightest cluster galaxies within 15,000 km s⁻¹. However, the directions of the LP10K and LP94 flow vectors differ by $\sim 70^\circ$. When the LP10K likelihood analysis is done with the flow required to lie along the LP94 direction, $l = 343^\circ$, $b = 52^\circ$, the best-fit flow amplitude is only 150–200 km s⁻¹, much smaller than the 700 km s⁻¹ found by LP94, and the fit quality is much worse than for the velocity vectors quoted in the previous paragraph. Thus, the LP10K data set is inconsistent with the flow vector measured by LP94.

The LP10K flow vector is similar in amplitude and direction to the motion of the Local Group with respect to the CMB, and lies within $\sim 40^\circ$ of the flows measured in the local ($cz \lesssim 5000$ km s⁻¹) universe in the late 1980s and early 1990s by Lynden-Bell *et al.* (1988), Willick (1990), Mathewson *et al.* (1992), and Courteau *et al.* (1993), as well as those obtained from a recent POTENT analysis of the Mark III and SFI data sets by Dekel *et al.* (1998). This suggests that the local universe, including the LG, participates in the large-scale flow detected by the LP10K TF sample, which in turn is driven by density inhomogeneities on scales $\gtrsim 150h^{-1}$ Mpc. The fact that the LP10K full sample yields the same result as the ETR may hint that convergence to the CMB is not seen even at distances $\gtrsim 200h^{-1}$ Mpc.

The results presented in this paper do not, by themselves, clinch the case for the reality of very large scale bulk flow, because their significance level is only slightly above 2σ . However, the excellent agreement of the LP10K TF bulk flow with that recently measured by Hudson *et al.* (1998) from the SMAC survey of elliptical galaxies adds considerable weight to their plausibility. On the other hand, the LP10K and SMAC results differ sharply from those reported in recent months by Giovanelli *et al.* (1998a,b) and Dale *et al.* (1998), who argue from the SFI/SCI TF data set that convergence to the CMB frame is clearly detected beyond $60h^{-1}$ Mpc. Resolution of this discrepancy is an important task for the near future.

The parameters of the multiparameter TF relation introduced in Paper I were solved for simultaneously with the flow parameters, with the results largely unchanged. In particular, a surface brightness dependence of the TF relation was confirmed, with $v_{\text{rot}} \propto I_e^{0.13} L^{0.29}$. The analysis in this paper treated the various sources of TF scatter more carefully than did Paper I, with the result that the intrinsic scatter of the TF relation is more strongly constrained. It is found to be $\sigma_I = 0.28 \pm 0.07$ mag, a value which should be accounted for by successful models of galaxy formation.

The author acknowledges the support of NSF grant AST-9617188 and the Research Corporation, and thanks Paul Steinhardt, Mike Hudson, and Keith Thompson for valuable discussions.

REFERENCES

Abell, G.O., Corwin, H.G., & Olowin, R.P. 1989, *ApJS*, 70, 1 (ACO)

Bernstein, G.M., Guhathakurta, P., Raychaudhury, S., Giovanelli, R., Haynes, M.P., Herter, T., & Vogt, N.P. 1994, *AJ*, 107, 1962

Burstein, D., & Heiles, C. 1978, *ApJ*, 225, 40 (BH)

Burstein, D., & Heiles, C. 1982, *AJ*, 87, 1165

Courteau, S., Faber, S.M., Dressler, A., & Willick, J.A. 1993, *ApJ*, 412, L51

Dale, D.A., Giovanelli, R., Haynes, M.P., Scoggio, M., Hardy, E., & Campusano, L.E. 1997, *AJ*, 114, 455

Dale, D.A., Giovanelli, R., Haynes, M.P., Campusano, L.E., Hardy, E., & Borgani, S. 1998, *ApJ*, in press (astro-ph/9810467)

Dekel, A., Eldar, A., Kolatt, T., Yahil, A., Willick, J.A., Faber, S.M., Courteau, S., & Burstein, D. 1998, preprint (astro-ph/9812197)

Dressler, A., Faber, S.M., D., Burstein, D., Davies, R.L., Lynden-Bell, D., Terlevich, R.J., and Wegner, G. 1987, *ApJ*, 313, L37

Giovanelli, R., Haynes, M.P., Wegner, G., da Costa, L.N., Freudling, W., & Salzer, J.J. 1996, *ApJ*, 464, L99

Giovanelli, R., Haynes, M.P., Freudling, W., da Costa, L.N., Salzer, J.J., & Wegner, G. 1998a, *ApJ*, 505, L91

Giovanelli, R., Haynes, M.P., Salzer, J.J., Wegner, G., da Costa, L.N., & Freudling, W. 1998b, *AJ*, in press (astro-ph/9808158)

Han, M.-S., & Mould, J.R. 1992, *ApJ*, 396, 453

Holzapfel, W.L., Ade, P.A.R., Church, S.E., Mauskopf, P.D., Rephaeli, Y., Wilbanks, T.M., & Lange, A.E. 1997, *ApJ*, 481, 35

Hudson, M.J., Smith, R.J., Lucey, J.R., Schlegel, D.J., & Davies, R.L. 1998a, in *Evolution of Large-Scale Structure: from Recombination to Garching*, Proceedings of the MPA/ESO Cosmology Conference

Hudson, M.J., Smith, R.J., Lucey, J.R., Schlegel, D.J., & Davies, R.L. 1998b, *ApJ*, submitted

Jorgensen, I., Franx, M., & Kjaergaard, P. 1996, *MNRAS*, 280, 167

Kogut, A. et al. 1993, *ApJ*, 419, 1

Lauer, T.R., & Postman, M. 1994, *ApJ*, 425, 418 (LP94)

Lynden-Bell, D., Faber, S.M., Burstein, D., Davies, R.L., Dressler, A., Terlevich, R., & Wegner, G. 1988, *ApJ*, 302, 536

Mathewson, D. S., Ford, V. L., & Buchhorn, M. 1992, *ApJS*, 81, 413

Paczynski, B., & Piran, T. 1990, *ApJ*, 364, 341

Perlmutter, S., et al. 1998, *ApJ*, in press (astro-ph/9812133)

Postman, M., & Lauer, T.R. 1995, *ApJ*, 440, 28

Postman, M., Huchra, J.P., & Geller, M.J. 1992, *ApJ*, 383, 404

Riess, A.G., Press, W.H., & Kirshner, R.P. 1995, *ApJ*, 445, L91

Riess, A.G., Davis, M., Baker, J., & Kirshner, R.P. 1997, *ApJ*, 488, L1

Riess, A.G., et al. 1998, *AJ*, 116, 1009

Saglia, R.P., Colless, M., Burstein, D., Davies, R.L., McMahan, R.K., Watkins, R., & Wegner, G. 1998, in *Evolution of Large-Scale Structure: from Recombination to Garching*, Proceedings of the MPA/ESO Cosmology Conference

Schlegel, D., Finkbeiner, D.P., & Davis, M. 1998, *ApJ*, 500, 525 (SFD)

Steinmetz, M., & Navarro, J. 1998, preprint (astro-ph/9808076)

Strauss, M.A., Cen, R., Ostriker, J.P., Lauer, T.R., & Postman, M. 1995, *ApJ*, 444, 507

Strauss, M. A., & Willick, J. A. 1995, *Phys. Rep.*, 261, 271

Struble, M.F., & Rood, H.J. 1991, *ApJS*, 77, 363

Wegner, G. et al., 1996, *ApJS*, 106, 1

Wegner, G. et al., 1998, *MNRAS*, in press

Willick, J. A. 1990, *ApJ*, 351, L5

Willick, J. A., Courteau, S., Faber, S. M., Burstein, D., & Dekel, A. 1995, *ApJ*, 446, 12

Willick, J. A., Courteau, S., Faber, S. M., Burstein, D., Dekel, A., & Strauss, M. A. 1997a, *ApJS*, 109, 333

Willick, J.A., Strauss, M.A., Dekel, A., & Kolatt, T. 1997b, *ApJ*, 486, 629

Willick, J.A. 1999a, *ApJ*, 516, 000, in press (Paper I; astro-ph/9809160)

Willick, J.A. 1999b, in preparation (Paper III)